JOURNAL OF GEOPHYSICAL RESEARCH, VOL. 107, NO. A10, 1285, doi:10.1029/2001JA009223, 2002

Correction published 21 December 2002

Electrostatic electron cyclotron waves generated by low-energy electron beams

J. D. Menietti, O. Santolik,[1,2] J. D. Scudder, J. S. Pickett, and D. A. Gurnett
Department of Physics and Astronomy, University of Iowa, Iowa City, Iowa, USA

Received 19 December 2001; revised 31 January 2002; accepted 28 February 2002; published 10 October 2002.

[1] We report the results of an investigation of waves observed by the Polar spacecraft at high altitudes and latitudes and at frequencies just above the cyclotron frequency. These observations are made frequently when the spacecraft is over the polar cap as well as near the dayside cusp and the nightside auroral region and for ratios of gyrofrequency to plasma frequency, $f_p/f_g \sim 1$. We investigate the role of electron beams with E $\lesssim$ 1 keV in the generation of these waves. Observed plasma parameters are used as input to a modification of the Waves in Homogeneous, Anisotropic Multi-component Plasmas (WHAMP) computer code to place constraints on the free energy source and growth of these waves. We conclude these waves are an indicator of the presence of low-energy electron beams and a cold electron component (E $\lesssim$ 0.2 eV) in regions with $f_p/f_g \lesssim 1$.
INDEX TERMS: 2780 Magnetospheric Physics: Solar wind interactions with unmagnetized bodies; 2459 Ionosphere: Planetary ionospheres (5435, 5729, 6026, 6027, 6028); 5440 Planetology: Solid Surface Planets: Magnetic fields and magnetism; 2728 Magnetospheric Physics: Magnetosheath; *KEYWORDS:* electrostatic electron waves, plasma waves, beam mode

Citation: Menietti, J. D., O. Santolik, J. D. Scudder, J. S. Pickett, and D. A. Gurnett, Electrostatic electron cyclotron waves generated by low-energy electron beams, *J. Geophys. Res.*, *107*(A10), 1285, doi:10.1029/2001JA009223, 2002.

1. Introduction

[2] Electrostatic electron cyclotron waves (EEC) have been studied for many years [cf. *Mosier et al.*, 1973; *Kurth et al.*, 1979a, 1979b]. The observations have typically been obtained during crossings of the plasmasheet near the magnetic equator, where the ratio of plasma frequency, f_p, to gyrofrequency, f_g, is typically much larger than 1, and where electron pitch angles are large. Intense noise bands are frequently observed in the plasmasphere at frequencies between f_p and the upper hybrid frequency, $f_{UH} = \sqrt{(f_p^2 + f_g^2)}$ [*Mosier et al.*, 1973]. Original numerical studies have shown that highest growth rates occur for $f_p/f_g > 1$ [cf. *Tataronis and Crawford*, 1970a, 1970b]. Bernstein mode waves [*Bernstein*, 1958] can grow, however, for both large and small ratios f_p/f_g [cf. *Krall and Trivelpiece*, 1973], and the ratio f_p/f_g determines the precise location of the emission fundamental and harmonic frequencies. *Young et al.* [1973] have shown that a dense, warm electron distribution of electrons with $df/dv_\perp > 0$ can excite waves with $f_g < f < 1.5\ f_g$ and, for $k_\parallel \neq 0$, a temperature anisotropy $T_\perp > T_\parallel$ can excite waves between f_g and $2f_g$. More recent investigations of electron cyclotron waves generated by beams and temperature anisotropies have been conducted for $f > f_g$ [*Winglee et al.*, 1992] and for $f < f_g$ [*Wong and Goldstein*, 1994].

[3] *Gurnett et al.* [1983] have reported "3/2 f_g" emission in the cusp in the DE 1 plasma wave data at a radial distance of about 3.5 R_E, at a time when $f_p/f_g \lesssim 1$. *Farrell et al.* [1990] subsequently studied a number of examples of wave intensifications near the cusp for $f \gtrsim f_g$. They found that the waves most often occurred at times of large magnetic index, *Kp*. For specific cases, these authors found the waves to be oblique with wave normal angles varying from $\theta \sim 10°$ to $\theta \sim 60°$. The electric field intensity of these waves was typically of the order of a few to tens of μV/m, much smaller than the large amplitude (n + 1/2) f_g oscillations observed by *Kurth et al.* [1979a, 1979b] inside the plasmasphere.

[4] *Menietti et al.* [2001] reported observations of EEC waves made by the Polar spacecraft as it traversed the northern polar magnetosphere at altitudes from approximately 7 R_E to 9 R_E. At these altitudes $f_p \sim f_g$ and the EEC waves were observed at a relatively narrow-banded emission at frequencies just above f_g. The apogee of the Polar spacecraft over the northern polar cap during 1996 and 1997, was approximately 9 R_E, and the spacecraft often entered a region where $f_p \gtrsim f_g$, because the gyrofrequency falls off more rapidly with radial distance than the plasma frequency. The waves are observed near the cusp, polar cap, and both dayside and nightside auroral regions. The wave intensities were frequently on the order of 0.1 mV/m, and the measured wave normal angles varied, but could be quite large (>60°). The EEC waves may be an indicator of the presence of electron beams wherever they are observed. Since the waves are not confined to any special region of the magnetosphere, and are seen on large portions of many northern hemisphere passes, the source of the electron beams becomes an interesting question.

[1] Now at Faculty of Mathematics and Physics, Charles University, Prague, Czech Republic.
[2] Also at Institute of Atmospheric Physics, Czech Academy of Sciences, Prague, Czech Republic.

0148-0227/02/2001JA009223$09.00

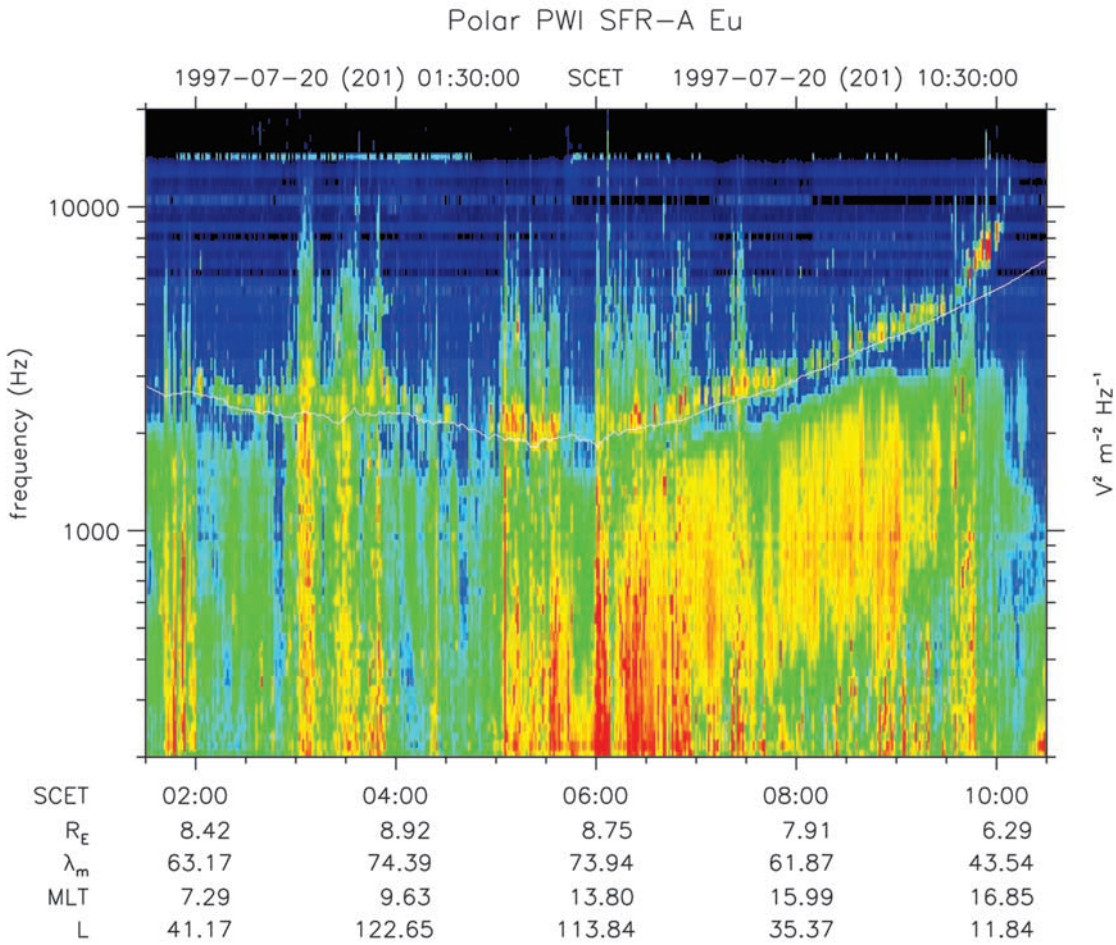

Figure 1. Frequency versus time spectrogram showing the emissions in question as an often intense (yellow and red), relatively narrowband feature just above the gyrofrequency (white line). This survey plot covers 9 hours of day 97/07/20 (day 201).

[5] In this paper we investigate electrostatic electron cyclotron wave growth using a modification of the Waves in Homogeneous, Anisotropic Multi-component Plasmas computer code (WHAMP) [*Rönnmark*, 1982]. We show that low-energy electron beams often seen associated with the waves, in the presence of a cold core plasma population can provide the free energy source for wave generation. The question of the source of the electron beams is not addressed.

2. Instrumentation

[6] The Polar satellite was launched in late February 1996 into a polar orbit with apogee of about 8 R_E and a perigee of about 2.2 R_E. Polar is the first satellite to have 3 orthogonal electric antennas (E_u, E_v, and E_z), 3 triaxial magnetic search coils, and a magnetic loop antenna, as well as an advanced plasma wave instrument [*Gurnett et al.*, 1995]. This combination can potentially provide the polarization and direction of arrival of a signal without any prior assumptions.

[7] The Plasma Wave Instrument (PWI) on the Polar spacecraft is designed to provide measurements of plasma waves in the Earth's polar regions over the frequency range from 0.1 Hz to 800 kHz. Five receiver systems are used to process the data: a wideband receiver, a high-frequency waveform receiver (HFWR), a low-frequency waveform receiver, two multichannel analyzers, and a pair of sweep frequency receivers (SFR). For the high frequency emissions of interest here, the SFR and the HFWR are of special interest. The HFWR measures high resolution waveform data using three orthogonal electric field antennas and three triaxial magnetic search coils. With the 25 kHz filter the sampling rate is 71.43 kHz. The SFR has a frequency range from 24 Hz to 800 kHz in 5 frequency bands. The frequency resolution is about 3% at the higher frequencies. In the log mode a full frequency spectrum can be obtained every 33 s.

[8] The Electron and Ion Hot Plasma Instrument (HYDRA) [*Scudder et al.*, 1995] is an experimental three-dimensional hot plasma instrument for the Polar spacecraft. It consists of a suite of particle analyzers that sample the velocity space of electron and ions between $\sim$ 10 eV/q to 35 keV/q in three dimensions, with a routine time resolution of 0.5 s. The satellite has been designed specifically to study accelerated plasmas such as in the cusp and auroral regions.

3. Observations and Calculations

[9] In Figure 1 we show a frequency-versus-time spectrogram of the SFR for a 9-hour period on day 201 of 1997, when the Polar spacecraft was high over the polar cap and

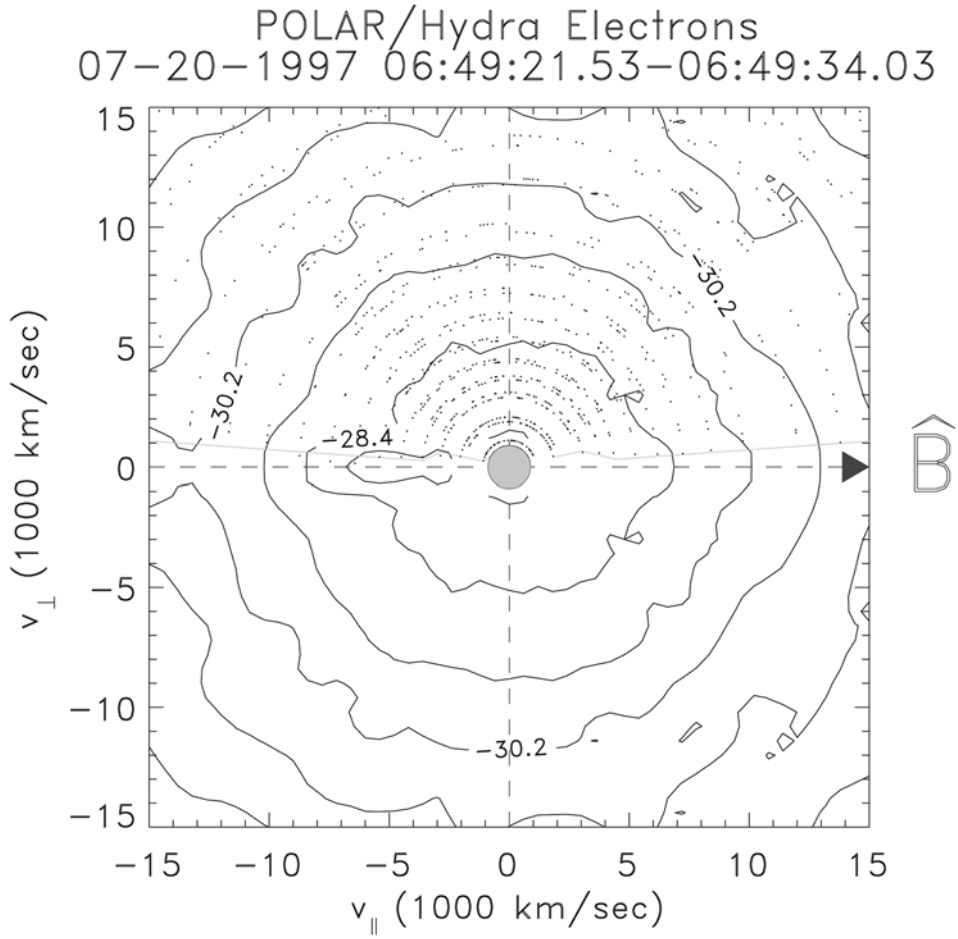

Figure 2. Contours of the velocity-space electron distribution function (s^3/cm^6) observed by HYDRA during a time period when electrostatic electron cyclotron waves were observed.

proceeded to the midafternoon auroral region. The frequency range shown is 200 Hz to 20 kHz. Clearly seen are whistler mode emission at frequencies $f < f_g$, where f_g is displayed by the white line. Also clearly seen are intense, highly electrostatic emissions in a relatively narrow band at frequencies just above f_g. Less intense, broadbanded electrostatic emission is often seen to extend well above f_g. *Menietti et al.* [2001] showed that these emissions are highly electrostatic and have no preferred polarization, consistent with a linear polarization measured by independent axial wave receivers on the spinning Polar spacecraft.

[10] In Figure 2 we plot contours of the electron distribution function in velocity space for a time period when electrostatic electron cyclotron waves were observed. The distribution is collected for a two-spin period of the Polar satellite. An electron beam with E < 1 keV is seen traveling up the field line away from Earth. It is clearly seen that the beam has a larger temperature parallel to the ambient magnetic field, $T_{\|}$, compared to the perpendicular temperature, $T_{\perp}$. During this time period the electron cyclotron frequency, f_g = 2200 Hz as measured by the magnetometer on board Polar, and the plasma frequency, f_p = 2520 Hz as determined from integration of the particle data from the hot plasma instrument (HYDRA). It is important to note that during the time of the observations reported in this paper, the plasma wave instrument indicated that $f_p \gtrsim f_g$, and thus the wave data could not be used to obtain the plasma density [cf. *Menietti et al.*, 2001]. The beam in Figure 2 is a typical electron beam seen during the time of the wave observations shown in Figure 1. Electron beams with E < 1 keV and varying temperatures are observed throughout the period of Figure 1 [cf. *Menietti et al.*, 2001, Figure 4].

[11] In order to investigate the role of these electron beams in the generation of the EEC waves, we have used a modification of a well-tested computer code WHAMP [*Rönnmark*, 1982]. WHAMP is a computer program which solves the dispersion relation of waves in a magnetized plasma. The dielectric tensor is derived using the kinetic theory of homogeneous plasmas with Maxwellian velocity distributions. Up to six different plasma components can be included (we use up to three in this work), and each component is specified by its density, temperature, particle mass, anisotropy and drift velocity along the magnetic field.

[12] In this study a modified form of the distribution function introduced by *Rönnmark* [1982, 1983] is used as follows:

$$f(v_{\perp}, v_{\|}) = \left\{ \frac{n_1}{\pi^{3/2} w_{\perp_1}^2 w_{\|_1}} \right\} e^{\frac{(v_{\|} - v_d)^2}{w_{\|_1}^2}} e^{-v_{\perp_1}^2 / w_{\perp_1}^2}, \qquad (1)$$

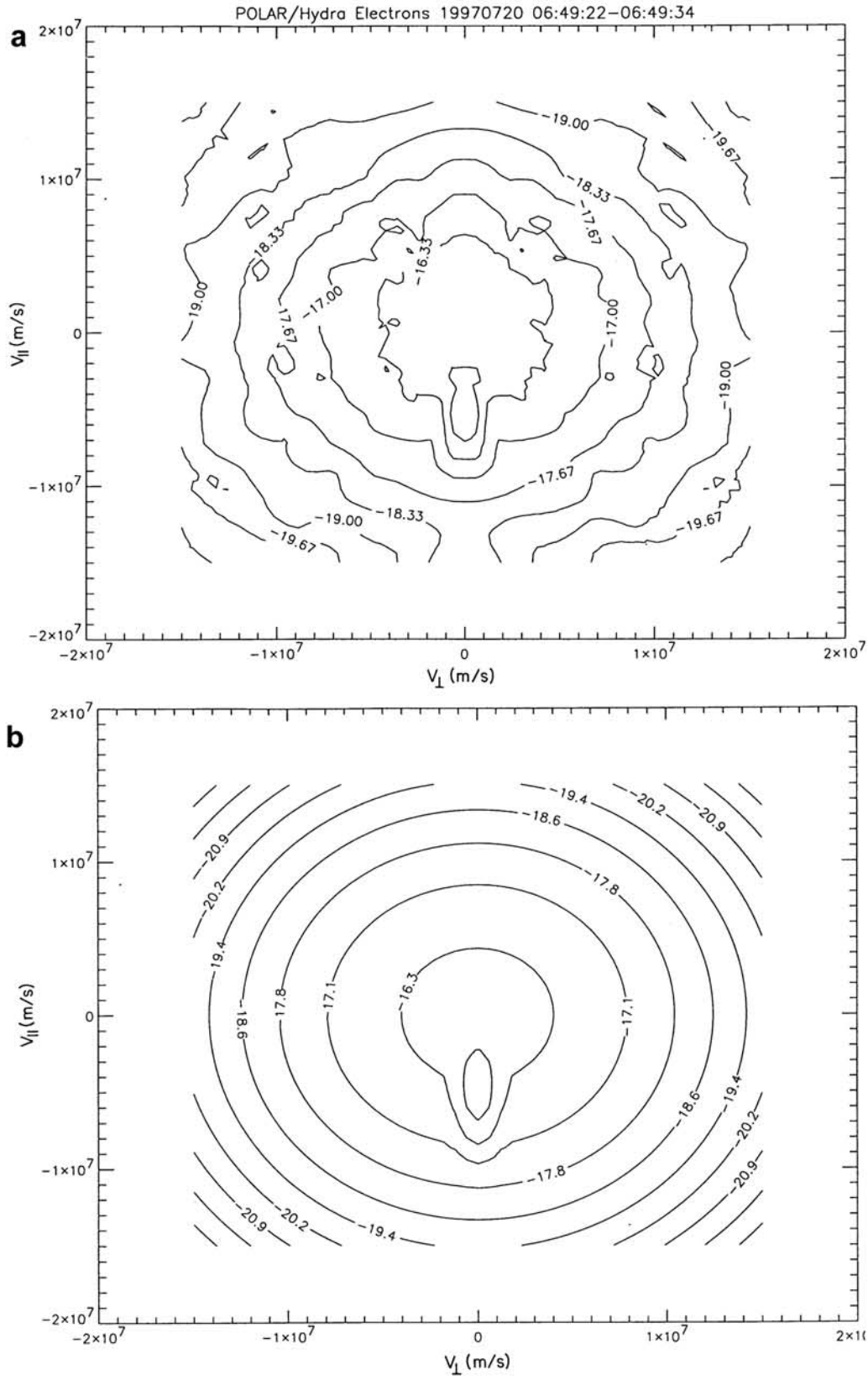

Figure 3. Contours of the velocity-space electron distribution function (s^3/m^6) resulting from a model of drifting Maxwellians equation (1). The fitting parameters are listed in Table 1.

Table 1. Fitting Parameters for Observed Electron Distribution

Background Maxwellian	Drifting Maxwellian
$T_{\|}$ = 170.5 eV	$T_{\|}$ = 27.9 eV
n_{bg} = 94%	n_{beam} = 6%
$T_{\perp}/T_{\|}$ = 0.87	$T_{\perp}/T_{\|}$ = 0.11
E_{drft} = 0	E_{drft} = 61.6 eV

where $v_{\|}$ and $v_{\perp}$ are the particle velocities parallel and perpendicular to the magnetic field, respectively; w_{-1} and w_{-1} are the parallel and perpendicular thermal velocities, respectively; v_d is the parallel drift velocity, and n_l is the density of the "l"th plasma component.

[13] We have tested our version of the WHAMP code by comparing the numerical and analytical results for the Langmuir, Bernstein, and ion acoustic modes assuming Maxwellian or drifting Maxwellian particle distributions. The dispersion curve and the growth rates were in excellent agreement.

[14] *Crawford* [1965] has derived the dispersion relation for electrostatic electron cyclotron waves in a warm plasma assuming a ring-beam distribution as well as an isotropic Maxwellian distribution. He shows the dispersion curves for these cases and comments that for the Maxwellian distributions the system is absolutely stable. However, for the ring-beam distribution given as

$$f = \frac{n}{2\pi_{v_R}}\delta(w_{\perp} - v_R)\delta(w_{\|} - v_d), \qquad (2)$$

unstable wave growth can occur for waves near perpendicular propagation and for larger values of f_p/f_g. In equation (2), v_R is the common speed of gyration about the field lines. The dispersion relation for arbitrary wave normal angles relative to the magnetic field is given by equation (22) of *Crawford* [1965]. We have found the roots of this equation and compared them to the results of more realistic distribution functions obtained using WHAMP as discussed below. For beam velocities similar to those used in the calculations below, the results of WHAMP compare well with those obtained from equation (22) of *Crawford* [1965].

[15] To begin our investigation we fit the distribution function of Figure 2 using a nonlinear leasts squares fitting routine. In Figure 3a we have replotted Figure 2 by rotating the figure and using units of s^3/m^6 for the distribution function. In Figure 3b we show the model fit consisting of a background and a drifting Maxwellian with fitting parameters shown in Table 1. For this distribution and all others we will present f_p = 2.520 kHz and f_g = 2.2 kHz (f_{UH} = 3.35 kHz), and the total plasma density is n_{total} = 7.82 x 10^{-2} cm^{-3}, unless otherwise noted. While the fit is good, the distribution of Figure 3b is not unstable to the growth of electrostatic waves. It is possible that the waves are both Landau and cyclotron damped in the presence of the warm electron background population [cf. *Tataronis and Crawford*, 1970b]. However, a cold core electron population, not present in the distribution of Figure 3b, can have important influence on stability.

[16] *Farrell et al.* [1990] have shown that low-energy electron beams ($T_{beam}/T_{background} \sim 1$) with a cold background plasma are marginally unstable to EEC waves. *Young et al.* [1973] found that a dense warm distribution with either $df/dv_{\perp} > 0$ or a temperature anisotropy ($T_{\perp} > T_{\|}$) can excite waves for $k_{\|} \neq 0$ in the range $f_g < f < 2.0\, f_g$. We confirm some of these results using a modification of the WHAMP code by introducing a distribution function with 3 Maxwellian components as described in Table 2. The energy of the cold component is well below the low-energy cutoff of the HYDRA instrument. *Farrell et al.* [1990] note the importance of keeping the temperature of the cold component low to obtain growth of the EEC waves.

[17] We believe a cold electron background population can modify the warm plasma distribution sufficiently to drive a marginally stable population to instability. The importance of the cold background population has also been reported by *Grabbe* [1985] for the investigation of electrostatic waves due ion beams. *Grabbe* [1985] found that increasing the density of a cold background electron population increased the growth rate as well as the frequency of the unstable waves. One might also suspect that increasing the beam energy might drive the instability without the introduction of a cold component. As we discuss later, we found this latter approach was not sufficient to generate the EEC waves.

[18] In Figure 4 we plot a contour of the distribution function for the parameters of Table 2. This distribution contains a beam, but is obviously much broader in $(T_{\perp}/T_{\|})_{beam}$ than the observed distribution of Figure 2. In Figure 5 we show the results of calculations of the roots of the dispersion relation, for the parameters of Table 2, and for wave normal angle, $\theta = 50°$. The coordinate of the plot is wave number, $k(m^{-1})$, and the three-panels display the real frequency (bottom), the ratio of the wave magnetic field to electric field multiplied by the speed of light, cB/E (middle), and the ratio f_i/f_r of imaginary to real frequency (top). In the bottom panel we display the whistler mode (dotted line) which shows a magnetic component but is not a growing mode for this distribution. Also seen is an electrostatic beam mode (solid line) which does have an imaginary frequency and thus growth rate. This mode is dependent on the beam and lies between f_g and f_{UH} as indicated.

[19] We have determined that distributions quite similar to those observed (Figure 2) are also unstable to the beam mode. In Table 3 we display the plasma parameters yielding the contours of the distribution function that are essentially the same as Figure 3b. Compared to Table 1, we see that this distribution also contains a low density beam and the temperature anisotropy of the beam distribution is the same as observed. Table 3 also indicates a cold component that is necessary for the distribution to be unstable to the beam mode. The density proportions in parentheses correspond to $T_{\|cold}$ = 0.227 eV. This cold component would normally be invisible to the plasma instrument because $T_{\|cold} \ll E_{min}$, where E_{min} is the minimum energy of HYDRA, and $E_{min} \sim$

Table 2. Fitting Parameters for Electron Distribution With Large $(T_{\perp}/T_{\|})_{beam}$

Cold Maxwellian	Background Maxwellian	Drifting Maxwellian
$T_{\|}$ = 0.057 eV	$T_{\|}$ = 170.5 eV	$T_{\|}$ = 51.2 eV
n_{cold} = 37%	n_{bg} = 28%	n_{beam} = 35%
$T_{\perp}/T_{\|}$ = 1	$T_{\perp}/T_{\|}$ = 0.87	$T_{\perp}/T_{\|}$ = 9.0
E_{drft} = 0	E_{drft} = 0	E_{drft} = 61.5 eV

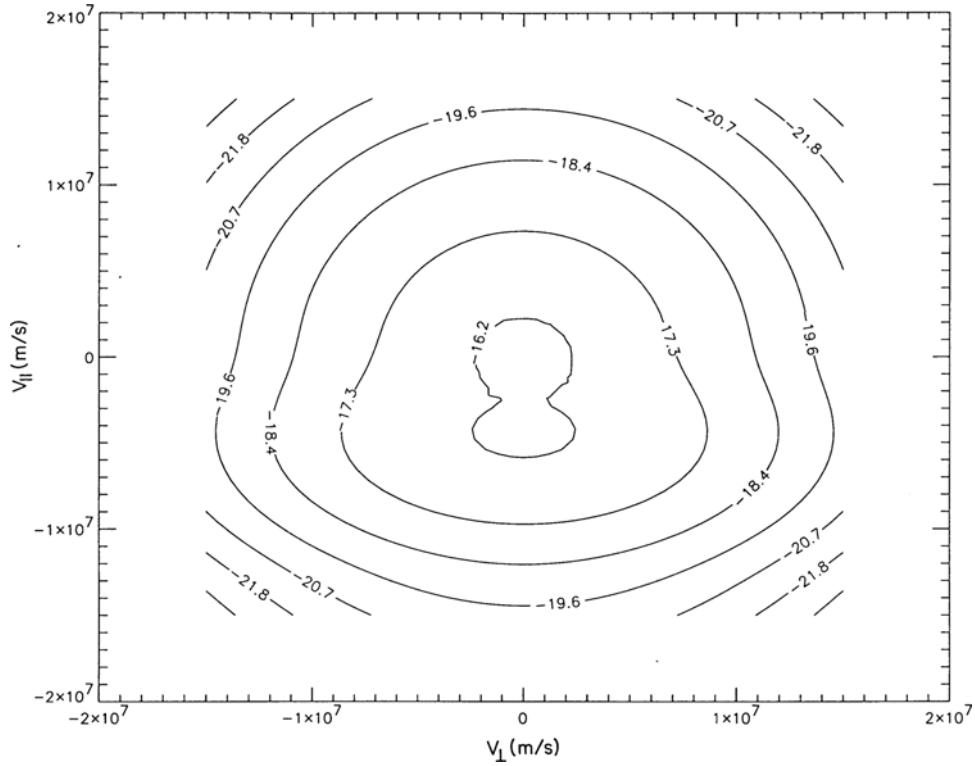

Figure 4. Same as Figure 3 but now for the fitting parameters of Table 2, which contain a cold background and a beam with a large temperature aniostropy, $(T_\perp/T_\parallel)_{\text{beam}} = 3$.

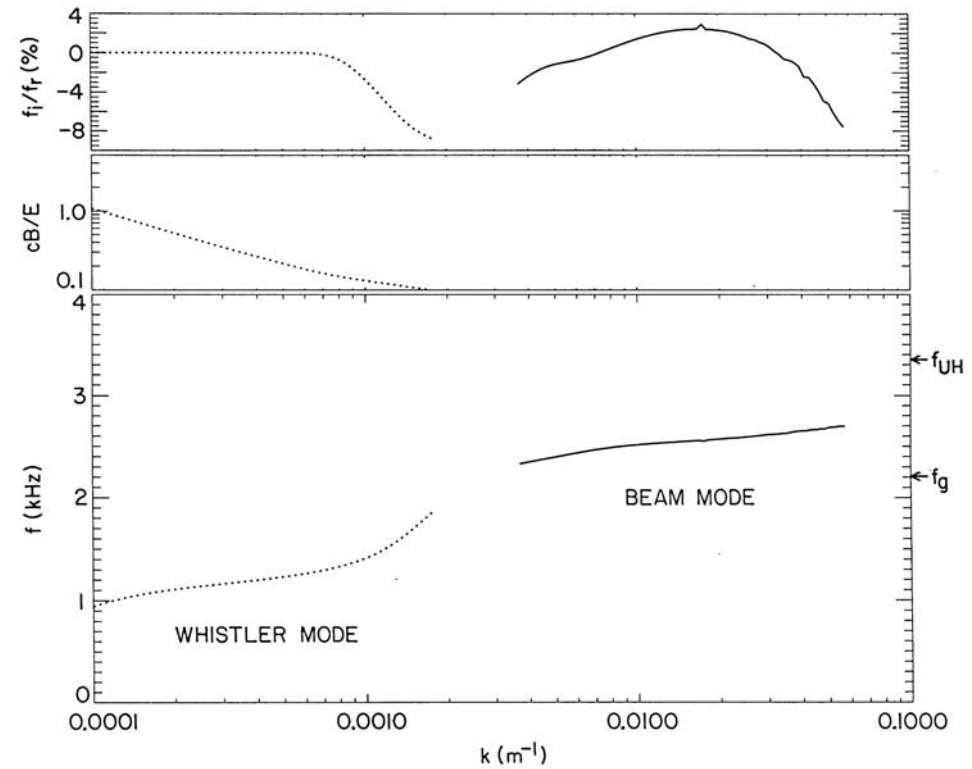

Figure 5. Results of the solution of the dispersion equation. The coordinate of the plot is wave number (m^{-1}) and the three panels display the real frequency (bottom), cB/E (middle), and the ratio f_i/f_r of imaginary to real frequency (top). In the bottom panel we display the nongrowing whistler mode (dotted line) and the electrostatic beam mode ($f_g < f < f_{UH}$), which does have a small but measurable imaginary frequency and thus growth rate.

Table 3. Fitting Parameters for Electron Distribution With Beam

Cold Maxwellian	Background Maxwellian	Drifting Maxwellian
$T_{\|}$ = 0.057 eV (0.227 eV)	$T_{\|}$ = 170.5 eV	$T_{\|}$ = 27.9 eV
n_{cold} = 20% (25%)	n_{bg} = 70% (65%)	n_{beam} = 10%
$T_{\perp}/T_{\|}$ = 1	$T_{\perp}/T_{\|}$ = 0.87	$T_{\perp}/T_{\|}$ = 0.11
E_{drft} = 0	E_{drft} = 0	E_{drft} = 61.6 eV

10 eV. However, it is believed that the spacecraft potential at time of Figure 2 is about $\varphi_{sc} \approx +23$ V. Thus we believe HYDRA is measuring all of the electrons, but any cold core component would be modified by the spacecraft potential and would still not be observed as a distinct population. In Figure 6 we plot the frequency versus wave number in the same format as Figure 5 for a wave normal angle of $\theta = 69°$ and the two different temperatures of the cold background, $T_{\|cold} = 0.227$ eV (dotted line) and $T_{\|cold} = 0.057$ eV (solid line). In Table 3 the density proportions of each species in parenthesis are for $T_{\|cold} = 0.227$ eV. A beam mode that is unstable to growth is present with $f_i/f_r \sim 6.6 \times 10^{-3}$, k = 1.59×10^{-2} m^{-1} ($T_{\|cold} = 0.227$ eV); and $f_i/f_r \sim 1.39 \times 10^{-2}$, k = 1.96×10^{-2} m^{-1} ($T_{\|cold} = 0.057$ eV). The real frequencies lie in the range $f_g < f < f_{UH}$, where they are observed. When the beam is removed, f_i becomes negative and thus damped as expected for the beam mode. We find the waves grow only for a fairly narrow range of large wave normal angles. For $T_{\|cold} = 0.057$ eV, this range was $50° \lesssim \theta \lesssim 75°$, and the largest growth occurred for $\theta \sim 69°$. Plots of f_i/f_r versus k for the range $50° \leq \theta \leq 75°$ are shown in Figure 7. For the case of $E_{cold} = 0.227$ eV, the group velocity, V_{gr}, over the range of maximum growth of the waves, $0.012 < k(m^{-1}) < 0.021$ is less than $\sim 3 \times 10^{-4}$ c, where c is the speed of light. The angle α, between $\mathbf{V}_{gr}$ and $\mathbf{B}$ near maximum growth is $\sim 22°$. For the case of $E_{cold} = 0.057$ eV, V_{gr}, over the range of maximum growth of the waves, $0.011 < k(m^{-1}) < 0.038$ is less than $\sim 1.5 \times 10^{-4}$ c, and $\alpha < 44°$ for k > 0.02 m^{-1}.

[20] The polarization of the emissions can be examined by plotting the time-tagged electric field components in field-aligned coordinates as was shown by *Menietti et al.* [2001]. However, after examining consecutive plots these authors found no consistent sense of polarization, rather there are about as many cases of apparent left hand as right hand polarization. This result is consistent with a linear polarization expected for electrostatic emission. The waves are measured independently from the three orthogonal antenna/receiver systems E_u, E_v, and E_z. A linear polarized wave will thus show a random phase difference between receivers for E_u and E_v, for instance. Thus we expect a random "circular" polarization as we observe, with no preferred handedness.

[21] We have further investigated the role of $T_{\|}$ in the growth of the observed waves. In Figure 8 we show contours of the velocity-space electron distribution function observed by HYDRA during a different time period of the same day when electrostatic electron cyclotron waves were observed near the dayside auroral region. The time period is

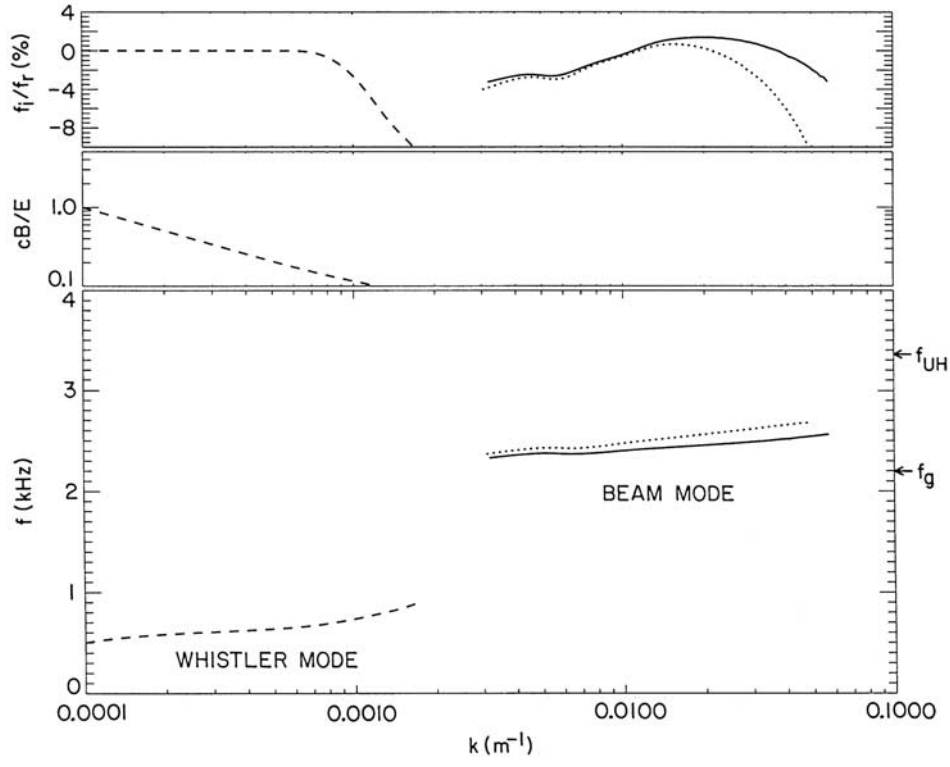

Figure 6. Frequency versus wave number in the same format as Figure 5. Note that a beam mode that is unstable to growth is present with $f_i/f_r \sim 1.4\%$ near $k = 2 \times 10^{-2}$. There are two curves for the beam mode, $T_{\|cold} = 0.227$ eV (dotted line) and = 0.057 eV (solid line). The real frequencies lie in the range $f_g < f < f_{UH}$, where they are observed.

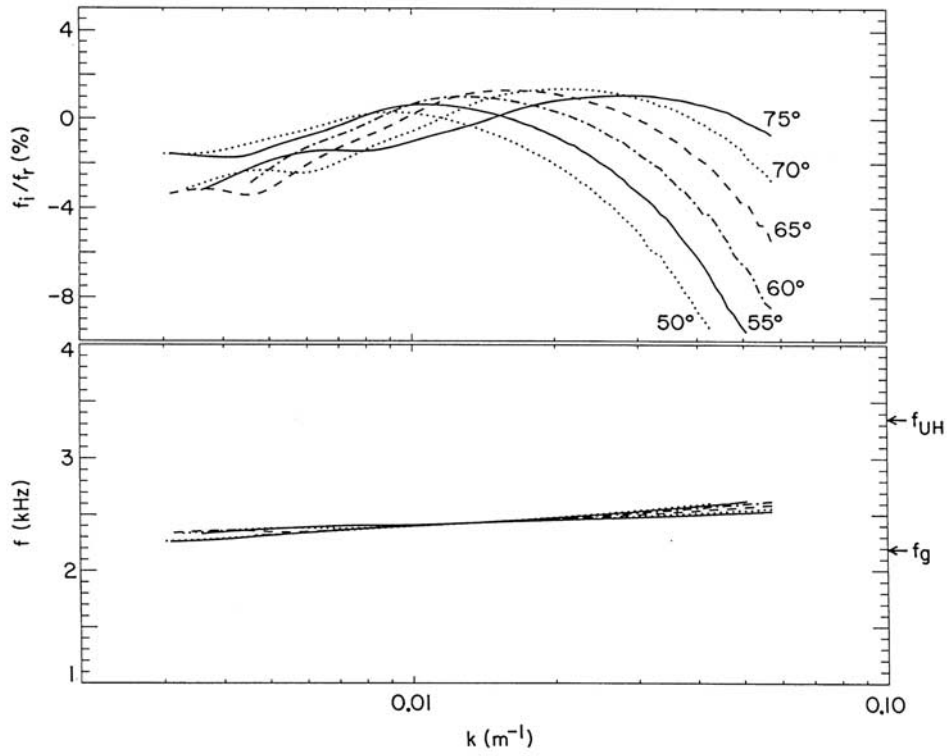

Figure 7. Plots of f_i/f_r versus k for the range of wave normal angles $50° \lesssim \theta \lesssim 75°$ are shown for the case of $T_{\|cold}$ = 0.057 eV and other parameters as listed in Table 3.

several hours earlier than Figure 2, and the electron beam parallel temperature is about 19 times higher. In Table 4 we list the fitting parameters of three cases used to model the data of Figure 8. For two of these models we used a slightly higher value of plasma frequency f_p = 2816 Hz, consistent with the HYDRA data. We again comment that the cold distribution function is essentially invisible to the HYDRA instrument, being well below the low-energy limit of the instrument. However, we find that the cold component is again necessary along with the beam to obtain growth of the waves. In Figure 9 we plot the calculated real and imaginary frequencies. Of the two values of $T_{\|cold}$ mentioned above, growth occurred only for $T_{\|cold}$ = 0.057 eV, with a value of $f_i/f_r \sim 2.0 \times 10^{-3}$ near k $\sim$ 0.024 m^{-1}, and $\theta = 70°$ for case 1. These waves again grow in the range $f_g < f < f_{UH}$ as observed (f_{UH} = 3609 Hz). Near maximum growth rate, $V_{gr} \sim 1 \times 10^{-4}$ c and $\alpha \sim 23°$. For case 2 we have changed the relative densities of each plasma component, allowing a 30% cold core. The overall fit of the electron distribution function contour to the data is still good, owing to the uncertainties in the fitting due to the incomplete data set (gaps in velocity phase space). For this case we find a maximum value of $f_i/f_r \sim 4.3 \times 10^{-3}$ near k $\sim$ 0.031 m^{-1} and $\theta = 70°$. Near maximum growth rate $V_{gr} \sim 0.7 \times 10^{-4}$ c and $\alpha \sim 25°$. For case 3 we have used the same ratio of density for each plasma component as in case 1, but we have increased the plasma frequency to 4016 Hz (f_{UH} = 4579 Hz), thus doubling the measured value, but still consistent with densities in the immediate vicinity of the observations. The measured spacecraft potential at time of Figure 8 is much lower at about $\varphi_{sc} \sim$ 10eV, which is near the low-energy cutoff of HYDRA. It is possible therefore that a cold plasma population exists at this time that is not detectable by HYDRA. For this case we find a maximum value of $f_i/f_r \sim 1.1 \times 10^{-2}$ near k $\sim$ 0.039 m^{-1}; $V_{gr} \sim 0.7 \times 10^{-4}$ and $\alpha \sim 15°$. These results are consistent with the general finding that larger ratios of f_p/f_g lead to stronger growth rates for the electrostatic electron cyclotron waves.

4. Summary and Discussion

[22] We have presented calculations of the dispersion function for an electron distribution containing a low-energy, low-temperature beam. Our calculations are performed using a modification of the WHAMP computer code for anisotropic plasmas that can be described by summed Maxwellian distributions with drifts and temperature anisotropies [*Rönnmark*, 1982]. We find that using electron distributions very similar those observed near the wave observations, we obtain a moderate wave growth of waves in the frequency range, $f_g < f < f_{UH}$ as observed.

[23] The electron distributions (measured by HYDRA) are associated with electron cyclotron waves observed by PWI as intense narrowbanded emissions at frequencies near and above the local gyrofrequency. These observations have been reported in the past for DE 1 wave data by *Farrell et al.* [1990] and for the Polar wave data by *Menietti et al.* [2001]. The waves have been observed often by the Polar spacecraft plasma wave instrument near the dayside auroral region, polar cap, and nightside auroral region for northern hemisphere passes when the satellite altitude is such that $f_g \lesssim f_p$. The electric fields are often nearly perpendicular to the

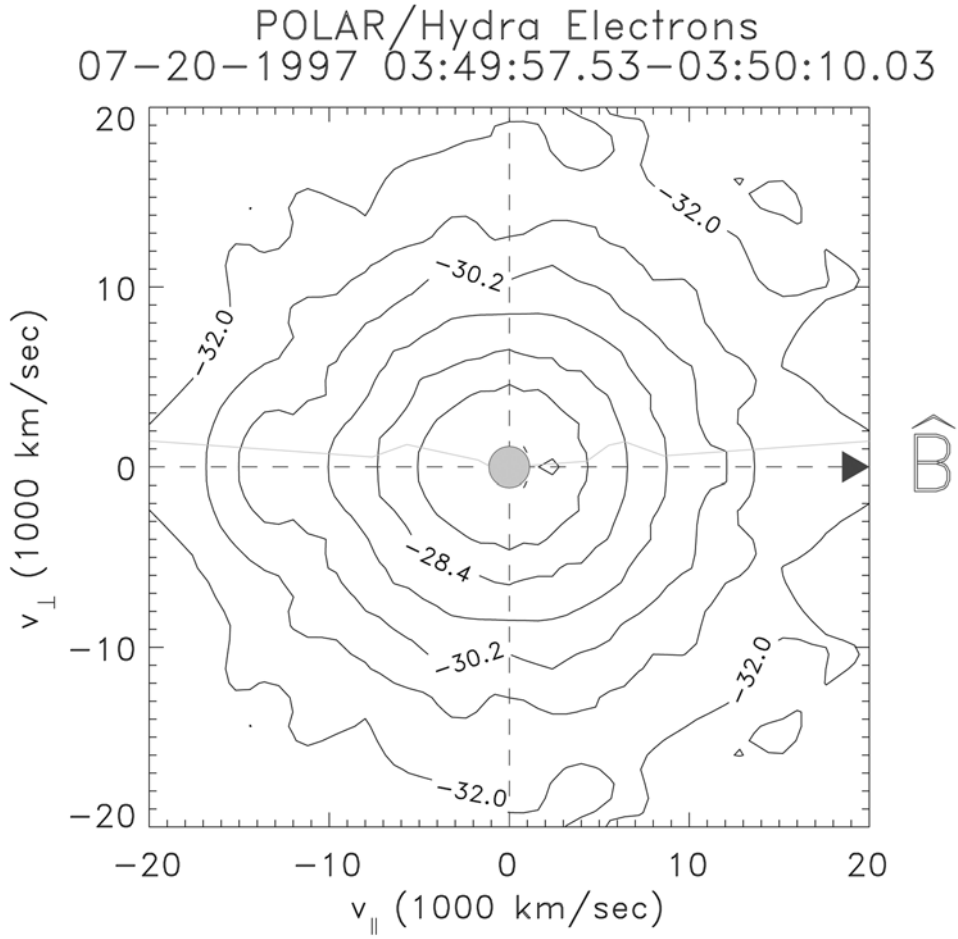

Figure 8. Contours of the velocity-space electron distribution function (s^3/cm^6) observed during a time period when electrostatic electron cyclotron waves were observed. The time period is several hours earlier than Figure 2, and the electron beam energy and parallel temperature are higher. The measured electron density is also somewhat higher.

ambient magnetic field. There are weak, if any, oscillations of the magnetic field present. The polarization measurements are consistent with a linear polarization.

[24] *Menietti et al.* [2001] reported an association of these observations with low-energy electron beams. These results are therefore consistent with *Farrell et al.* [1990] who observed a correlation of similar waves seen in the cusp with beaming electrons with energies of a few hundred eV. These latter authors indicated that electron distributions containing low-energy beams with $T_{beam}/T_{background} \sim 1$ and $f_p/f_g \sim 1.28$ were mildly unstable to the growth of the waves. For the latter study the beam was relatively high density with the ratio of $n_{beam}/n_{total} = 0.35$. Our studies indicate that the observed electron distributions, which we believe are typical of those made by PWI on northern hemisphere passes of the Polar spacecraft, contain temperature anisotropies with $(T_\perp/T_\parallel)_{beam} \sim 0.1$. For low-energy electron beams with $(T_\perp/T_\parallel)_{beam} \sim 0.1$ in the presence of a warm background and a cold core electron distribution, the plasma is unstable to the growth of electrostatic waves in the observed frequency range ($f_g < f < f_{UH}$). For our case the beams are relatively low density, with $n_{beam}/n_{total} \sim 0.10$ and growth rates are comparable to but somewhat smaller than those expected from the weak beam approximation. We conclude that the observed low-energy electron beams are the probable free-energy source of the observed electrostatic electron cyclotron waves. Referring again to equation (22) of *Crawford* [1965], for the ring-beam distribution as well as his equation (25) for an isotropic Maxwellian distribution, the electron velocity dispersion relations both have a resonance when

$$(\omega k_\parallel v_d)^2 (\omega_g)^2 = 0 \tag{3}$$

where $\omega = 2\pi f$. We therefore believe the instability in our numerical results involves both the cyclotron and Cerenkov resonance terms.

Table 4. Fitting Parameters for Electron Distribution With Higher Beam Temperature

	Cold Maxwellian	Background Maxwellian	Drifting Maxwellian
	$T_\parallel = 0.057$ eV	$T_\parallel = 451$ eV	$T_\parallel = 532$ eV
	$T_\perp/T_\parallel = 1$	$T_\perp/T_\parallel = 1.12$	$T_\perp/T_\parallel = 0.164$
	$E_{drft} = 0$	$E_{drft} = 0$	$E_{drft} = 57.6$ eV
Case 1	$n_{cold} = 20\%$	$n_{bg} = 65\%$	$n_{beam} = 15\%$
Case 2	$n_{cold} = 30\%$	$n_{bg} = 55\%$	$n_{beam} = 15\%$
Case 3	$n_{cold} = 20\%$	$n_{bg} = 65\%$	$n_{beam} = 15\%$

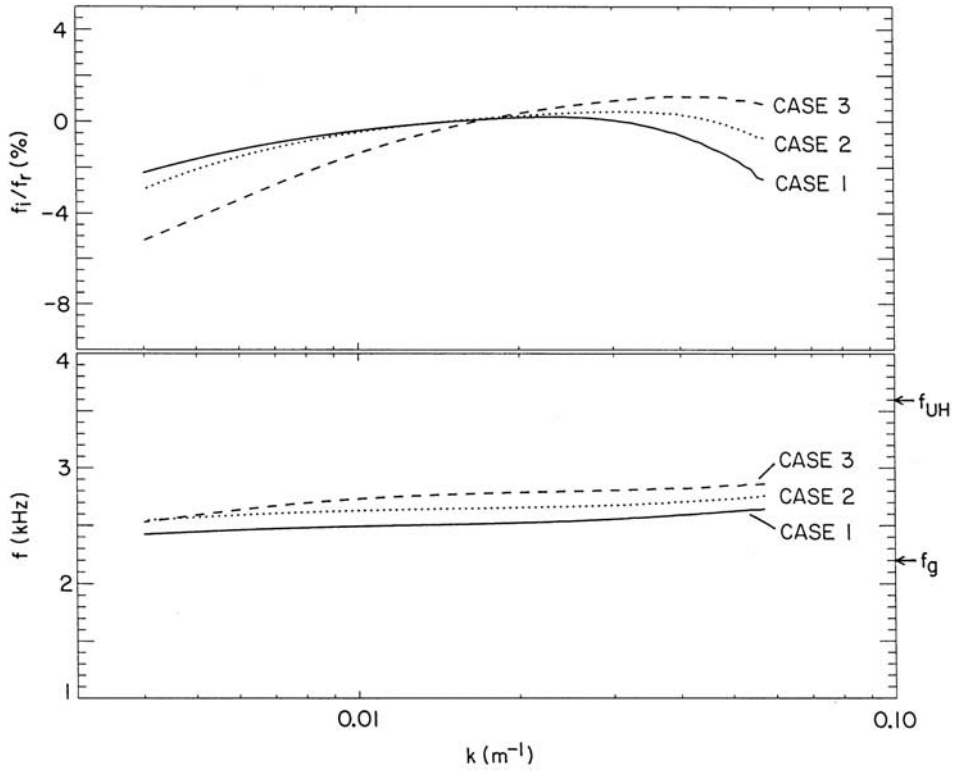

Figure 9. Plots of f_i/f_r in the same format as Figure 5 but now for the three cases of plasma parameters listed in Table 4 (to approximate the distribution shown in Figure 8). Note that $f_i/f_r > 0$ for each case indicating a positive growth rate for the waves in the frequency range $f_g < f < f_{UH}$, consistent with the observations.

[25] Following the example of past investigators we have introduced a cold background population of electrons to help drive the instability. We mention here that before we pursued this approach, we also tried increasing the drift velocity assuming that we were observing a beam that had already been modified by a wave-particle interaction. We found, however, that modest increases in the drift velocity of up to 2 times the energy did not produce wave growth. However, if we additionally added a cold background electron component, we obtained growth rates about 50% higher than corresponding growth rates for lower energy beams.

[26] Our investigation has been limited to linear theory and we have not investigated the nonlinear saturation of the waves and corresponding power levels expected from the growth rate calculations. Furthermore, while we have stated some general requirements for the density and energy of the cold core plasma, no precise density or energy limits have been placed on this population due to uncertainties in fitting the observed electron distribution function. These uncertainties result from a lack of particle data for $E \lesssim 10$ eV and from modifications of the original distribution due to spacecraft charging potentials. We have found that reasonable growth of the waves occurs for a cold core population that is greater than about 20% of the total population and with a thermal energy of $\lesssim 0.2$ eV. It will be important for future investigators to place better limits on the cold plasma population.

[27] **Acknowledgments.** We thank J. Faden for formatting the HYDRA data and J. Hospodarsky for text editing. This work was supported under grants NAG5-7943, NAG5-9561, and NAG5-8119 with NASA/Goddard Space Flight Center. O. Santolik thanks the Fulbright Commission in Prague for support during his stay at Iowa.

[28] Shadia Rifai Habbal thanks Donald B. Melrose and William M. Farrell for their assistance in evaluating this paper.

References

Bernstein, I. B., Waves in a plasma in a magnetic field, *Phys. Rev.*, *109*, 10–21, 1958.

Crawford, F. W., Cyclotron harmonic waves in warm plasmas, *Radio Sci.*, *69D*, 789–805, 1965.

Farrell, W. M., D. A. Gurnett, J. D. Menietti, H. K. Wong, C. S. Lin, and J. L. Burch, Wave intensifications near the electron cyclotron frequency within the polar cusp, *J. Geophys. Res.*, *95*, 6493–6504, 1990.

Grabbe, C. L., New results on the generation of broadband electrostatic waves in the magnetotail, *Geophys. Res. Lett.*, *12*, 483–486, 1985.

Gurnett, D. A., S. D. Shawhan, and R. R. Shaw, Auroral hiss, Z mode radiation, and auroral kilometric radiation in the polar magnetosphere: DE 1 observations, *J. Geophys. Res.*, *88*, 329–340, 1983.

Gurnett, D. A., et al., Polar plasma wave instrument, *Space Sci. Rev.*, *71*, 597–622, 1995.

Krall, N. A., and A. W. Trivelpiece, *Principles of Plasma Physics*, 674 pp., McGraw-Hill, New York, 1973.

Kurth, W. S., M. Ashour-Abdalla, L. A. Frank, C. F. Kennel, D. A. Gurnett, D. D. Sentman, and B. G. Burek, A comparison of intense electrostatic waves near f_{UHR} with linear instability theory, *Geophys. Res. Lett.*, *6*, 487–490, 1979a.

Kurth, W. S., J. D. Craven, L. A. Frank, and D. A. Gurnett, Intense electrostatic waves near the upper hybrid resonance frequency, *J. Geophys. Res.*, *84*, 4145–4164, 1979b.

Menietti, J. D., J. S. Pickett, D. A. Gurnett, and J. D. Scudder, Electrostatic electron cyclotron waves observed by the plasma wave instrument on board Polar, *J. Geophys. Res.*, *106*, 6043–6057, 2001.

Mosier, S. R., M. L. Kaiser, and L. W. Brown, Observations of noise bands associated with the upper hybrid resonance by the Imp 6 radio astronomy experiment, *J. Geophys. Res.*, *78*, 1673–1679, 1973.

Rönnmark, K., Waves in homogeneous, anisotropic, multi component plasmas, *Rep. 179*, Kiruna Geophys. Inst., Kiruna, Sweden, 1982.

Rönnmark, K., Computation of the dielectric tensor of a Maxwellian plasma, *Plasma Phys.*, *25*, 699–701, 1983.

Scudder J., et al., HYDRA-A 3-dimensional electron and ion hot plasma instrument for the Polar spacecraft of the GGS mission, *Space Sci. Rev.*, *71*, 459–495, 1995.

Tataronis, J. A., and F. W. Crawford, Cyclotron harmonic wave propagation and instabilities, I, Perpendicular propagation, *Plasma Phys.*, *4*, 231–248, 1970a.

Tataronis, J. A., and F. W. Crawford, Cyclotron harmonic wave propagation and instabilities, II, Oblique propagation, *Plasma Phys.*, *4*, 249–264, 1970b.

Winglee, R. M., J. D. Menietti, and H. K. Wong, Numerical simulations of bursty radio emissions from planetary magnetospheres, *J. Geophys. Res.*, *97*, 17,131–17,139, 1992.

Wong, H. K., and M. L. Goldstein, Electron cyclotron wave generation by relativistic electrons, *J. Geophys. Res.*, *99*, 235–240, 1994.

Young, T. S. T., J. D. Callen, and J. E. McCune, High-frequency electrostatic waves in the magnetosphere, *J. Geophys. Res.*, *78*, 1082–1099, 1973.

D. A. Gurnett, J. D. Menietti, J. S. Pickett, and J. D. Scudder, Department of Physics and Astronomy, University of Iowa, 203 Van Allen Hall, Iowa City, IA 52242-1479, USA. (jdm@space.physics.uiowa.edu)

O. Santolik, Charles University, KEVF MFF, V Holesovickach 2, Praha 8, CZ-1800, Czech Republic.